Available online at www.sciencedirect.com

ScienceDirect

Procedia Structural Integrity 57 (2024) 494–501

Structural Integrity Procedia

www.elsevier.com/locate/procedia

Fatigue Design 2023 (FatDes 2023)

Specimen design for gigacycle fatigue testing of structural steel welded joints

Andrew England[a]*, Athanasios Toumpis[a], Yevgen Gorash[a]

[a]*Department of Mechanical & Aerospace Engineering, University of Strathclyde, James Weir Building, 75 Montrose Street, Glasgow G1 1XJ, United Kingdom*

Abstract

Structures and components across a range of industries exhibit service lives above 10^7 cycles, but there is limited fatigue data in this domain. Conducting fatigue tests in the gigacycle regime is only feasible by using ultrasonic fatigue testing machines in which specimens are typically excited at 20 kHz. This research focuses on the design of a novel specimen which captures the geometric stress concentration at the weld toe, as an alternative to typically used cylindrical 'hourglass' shaped specimens. The gas-shielded flux-core arc welding method was used to manufacture butt joints of 080A15 structural steel. Specimens were tested in fully reversed axial loading at room temperature using a Shimadzu USF-2000A ultrasonic fatigue testing machine. Specimens failed in the range of 10^4-10^7 stress cycles with all fatigue cracks initiating at the weld toe. One specimen was classed as a run-out after being subjected to 3 x 10^9 stress cycles without failure. The fatigue data obtained was assessed using the effective notch stress method and showed similar fatigue performance to the IIW guidelines.

Keywords: Ultrasonic fatigue testing; Gigacycle fatigue; Welded joints

1. Introduction

It has been established that the assumption of a fatigue limit at 10^6-10^7 cycles is not valid for steels and their welded joints (Bathias & Paris, 2005). In applications across numerous industry sectors, the expected service life of welded components and structures of low carbon steel is in the gigacycle domain (10^9-10^{10} cycles), however there is a lack of

* Corresponding author. Tel.: +44-141-5484851
E-mail address: andrew.england@strath.ac.uk

10.1016/j.prostr.2024.03.054

experimental data and standards for this domain due to the testing time required (Fry, 2014). The development of ultrasonic fatigue testing (UFT) at a frequency of 20 kHz has enabled fatigue tests to 10^9 cycles to be completed in 14 hours. Using a conventional servohydraulic testing machine operating at 20 Hz, the same test would take 500 days (Kuhn & Medlin, 2000). With UFT, specimens are longitudinally vibrated at their natural frequency of 20 kHz, therefore the testing time and energy consumption are vastly reduced (Fitzka et al., 2021). The elevated frequency introduces issues with testing of low carbon steels, most notably the frequency effect, where an increase in fatigue strength compared to conventional fatigue tests is observed (Torabian et al., 2017). Due to the natural frequency and cooling requirements, 'hourglass' shaped specimens with a small minimum diameter are recommended by the standard WES 1112 (2022). This presents a challenge when assessing the fatigue performance of as-welded joints, as the machining required for these specimens eliminate the weld toe and root features that fatigue failures often originate from in components (Phillips, 2016).

Research on the gigacycle fatigue performance of low carbon steel welds is limited. Zhao et al. (2012) studied the fatigue strength of EH36 welds ground flush using UFT and found no fatigue limit below 10^{10} cycles, for both base material (BM) and welded specimens. In addition, it was observed that the fatigue strength of welded joints was significantly lower due to cracks initiating at pores and inclusions within the fusion zone (FZ). A similar decrease in fatigue strength in welded specimens was observed for 16Mn steel BM and welds using an hourglass specimen with an as-welded joint in the central gauge section (Liu et al., 2014). This study presents the design of a novel rectangular butt-welded specimen suitable for using UFT to investigate the gigacycle fatigue performance of low carbon steel flux-core arc welds.

2. Materials and methods

2.1. Materials

All test specimens were produced from 12 mm thick 080A15, a general purpose low carbon steel. The weld filler material used was 1.2 mm diameter low carbon steel flux-cored wire of type T 42 2 ZMn P M21 1 H5 (EN ISO 17362, 2015). The chemical composition of the BM and deposited weld electrode, per the material certificate and manufacturer's data sheet respectively, are shown in Table 1.

Table 1. Chemical composition of the base metal and as-deposited filler metal (%)

Material	C	Si	Mn	P	S
080A15	0.15	0.22	0.7	0.016	0.01
T 42 2 ZMn P M21 1 H5	0.05	0.41	1.36	0.010	0.008

The mechanical properties for 080A15 and deposited filler material, according to the material certificate and relevant standard are displayed in Table 2.

Table 2. Mechanical properties of base metal and as-deposited filler metal (EN ISO 17362, 2015)

Material	Yield strength (MPa)	Tensile strength (MPa)	Elongation (%)
080A15	357	467	23
T 42 2 ZMn P M21 1 H5	390 (min.)	500-640	20 (min.)

2.2. Welding procedure

As one of the aims of this work was to include the weld toe within the region of highest stress, a novel design was used where the weld was located in the centre of a 3 mm thick gauge section. Before welding, the 12 mm 080A15 plate sections were milled to the required profile. The plate sections were butt welded in the flat position, implementing a double-sided configuration where the joint was welded from each side. A semi-automated welding rig was utilised

which ensured the travel speed, alignment of the welding torch and contact tip to work distance (CTWD) were constant. The gas-shielded flux-core arc welding process was used, with 20% CO_2 / 80% Argon shielding gas. The welding parameters were consistent for each pass and are shown in Table 3. The current and voltage were recorded by a calibrated weld data logger. After each weld pass was complete, the solidified slag was removed by wire brush. The implemented welding parameters were determined from a series of test welds, altering the current, voltage, and travel speed.

Table 3. Welding parameters of FCAW process

Current (A)	Voltage (V)	Travel speed (mm/min)	Arc energy (J/mm)	CTWD (mm)	Root gap (mm)	Gas flow rate (l/min)	Torch angle
108-114	18.9-19.2	300	408-438	15	1.5	15	15º (drag)

2.3. Specimen design

Specimens were designed to have a longitudinal modal shape at a resonant frequency of 20 kHz by conducting modal analysis in Abaqus finite element analysis (FEA) software, as displayed in Fig. 1a . A fine mesh with 37145 C3D8R elements was used. The proportionality constant is required for calculating the displacement amplitude of a specimen for a given stress amplitude during ultrasonic loading (Swacha & Lipski, 2023). This was determined as 10.9 MPa/ µm using harmonic FEA with the same mesh as the previous modal analysis. The distribution of stress and displacement along the specimen axis is shown in Fig. 1b.

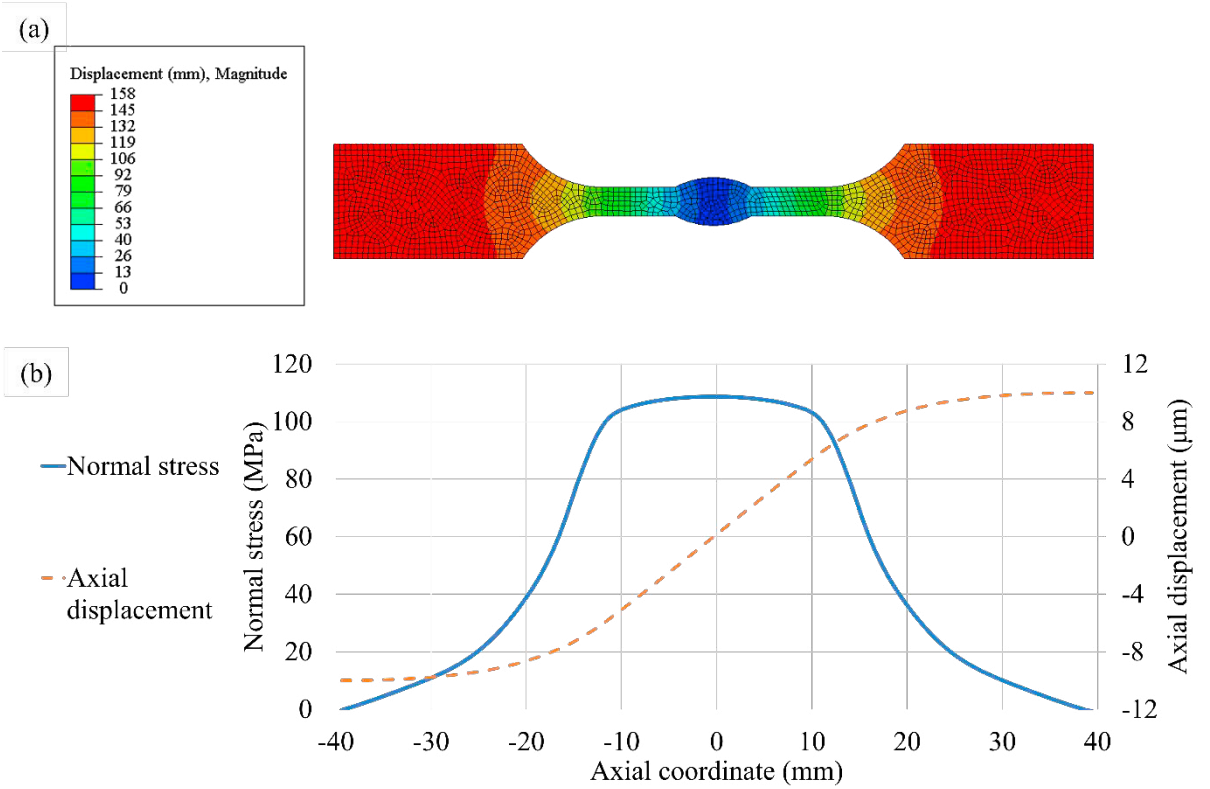

Fig. 1. Specimen design using FEA: (a) Mode shape at natural frequency of 20 kHz; (b) Axial stress and displacement during ultrasonic loading with vibration amplitude of 10 µm (neglecting stress concentration).

2.4. Experimental methods

Two metallography specimens were examined from the weld to assess weld quality and microstructure. Each specimen underwent the standard metallographic preparation procedure of mounting, grinding and polishing, before etching with 2% Nital. An Olympus light optical microscope was used to capture micrographs from each metallography specimen. The metallography specimens were subsequently used for Vickers microhardness testing using a Qness 60A+ with 0.5 kg load and 10 s dwell time. Microhardness measurements were taken in the BM, HAZ and FZ.

Fatigue test specimens were extracted from the welded plate by waterjet cutting, before having threads machined by turning, as shown in Fig. 2a. The specimens' sides were ground with fine grit paper to achieve a surface roughness less than 0.2 µm R_a (ISO 1099, 2017), verified by measurements using a Mitutoyo profilometer. The fatigue tests were conducted using a Shimadzu USF-2000A ultrasonic fatigue testing machine at a loading frequency of 20 kHz. The machine operates by converting an electrical signal into a mechanical displacement by a piezoelectric actuator. The displacement is amplified by a titanium horn with an internal thread used for attaching the specimens (Shimadzu, 2017). The USF-2000A was used in conjunction with a Shimadzu AG-X 5kN mean stress loading mechanism, but all tests were conducted at zero mean stress (R = -1).

Internal heat generation during loading is a significant challenge in UFT of ferritic steels (Pu et al., 2019). Therefore, specimens were cooled by compressed dried air supplied from three cooling nozzles, as shown in Fig. 2b. Additionally, intermittent driving was used where specimens were loaded for a short time, followed by a cooling pause. The surface temperature of the specimens was monitored using a high-speed pyrometer. The specimens were spray painted matt black in order to increase the surface emissivity and accuracy of the temperature readings (Gorash et al., 2023). The temperature of specimens was kept below 25°C throughout tests using the combination of cooling nozzles and intermittent driving. Crack propagation alters specimen geometry, resulting in a change in the natural frequency (Shimadzu, 2017). Once the natural frequency fell outside the range of 19.5 kHz to 20.5 kHz, the tests were automatically stopped by the built-in crack detection feature, and this was taken as the point of specimen failure. Specimens were loaded until failure or 3 x 10^9 loading cycles had been achieved. Failed specimens were pulled apart using a servohydraulic machine to reveal the crack propagation surface. Images of the fracture surface were captured using a digital camera with a high zoom macro lens.

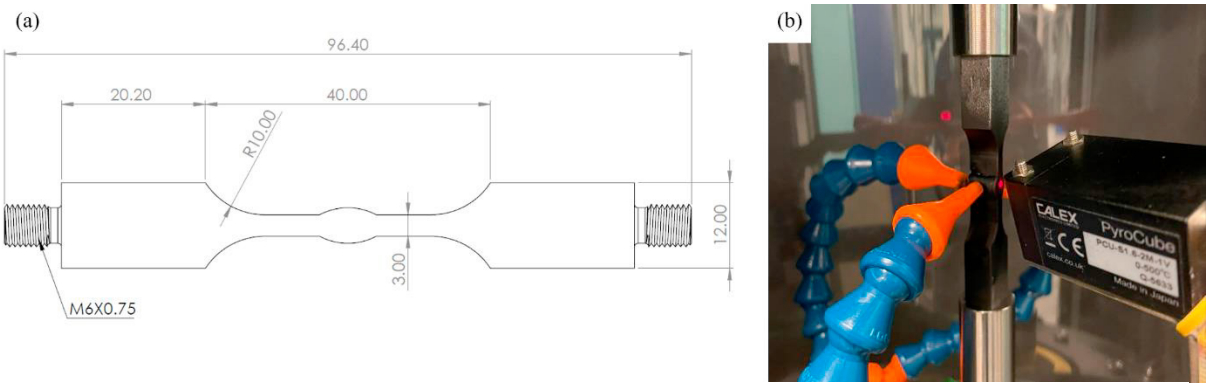

Fig. 2. (a) Main dimensions of ultrasonic fatigue specimen; (b) specimen attached to USF2000A with cooling nozzles and infrared pyrometer.

3. Results and discussion

3.1. Metallography and microhardness

The microstructure of the 080A15 BM (Fig. 3a) consists of equiaxed ferrite grains and distributed pearlite islands. This ferritic-pearlitic microstructure is typical for low-carbon steel (Benscoter & Bramfitt, 2004). The microhardness of this region is approximately 140 HV, the lowest measurement recorded in the metallography sample. The HAZ

displays a more complex microstructure which varied across its width. Fig. 3b illustrates a micrograph of the coarse-grained HAZ, close to the FZ. In this region the microstructure exhibits a significant distinction from the BM, consisting mainly of primary ferrite and bainitic ferrite. The greatest hardness value in the welded joint is found in the coarse-grained HAZ, at 279 HV. The FZ (Fig. 3c) is mostly comprised of idiomorphic ferrite (IF), and allotriomorphic ferrite (AF) formed at the prior austenite grain boundaries. The FZ exhibits a consistent hardness value of approximately 210 HV, due to the prevailing microstructure of fine grained IF. In general, the hardness values were similar to those found in welded joints of similar low carbon steels (Zhao et al., 2012).

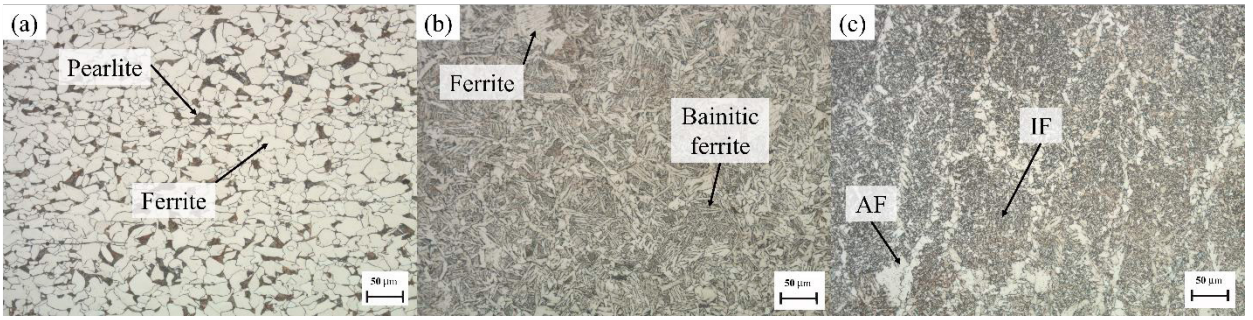

Fig. 3. Microstructure of (a) BM [x200, etched]; (b) HAZ [x200, etched]; (c) FZ [x200, etched].

3.2. Fatigue testing

The results of the five ultrasonic fatigue tests conducted are shown in Fig. 4. The nominal stress amplitude refers to the stress in the BM in the gauge section of the specimen, determined from the harmonic FEA model (Section 2.3). Four specimens exhibited fatigue failure at stress amplitudes from 320 MPa to 115 MPa. These data points were fitted to the classical Basquin (1910) equation:

$$\sigma_a = A{N_F}^B$$

where σ_a is the applied stress amplitude in MPa, N_f is the number of cycles to failure, and A and B are material parameters. The fitted curve is shown in Fig. 4 for a 50% survival probability with A = 1910 and B = -0.172. The experimental data shows little scatter and a good fit to the Basquin curve, with an R^2 value of 0.99. BS 7608 (2015) assumes an endurance limit at 1 x 10^7 cycles for steel welds. Notably, one specimen failed at a slightly greater number of cycles, N_f = 1.05 x 10^7, at an applied stress amplitude σ_a = 111 MPa. One specimen tested at 125 MPa was classed as a run-out after 3 x 10^9 stress cycles. During testing of this run-out specimen, there was no change in test frequency or a pronounced increase in specimen temperature, either of which indicate crack propagation. The number of tests conducted limit the applicability of the fatigue results for design purposes, but serve as a proof of concept of the specimen design.

The points in the SN curve show the number of cycles before the fracture detection feature was triggered and the test was automatically stopped. One specimen (σ_a = 200 MPa, N_f = 5.25 x 10^5) was subsequently cyclically loaded at the same stress amplitude on a conventional servohydraulic testing system at 20 Hz until fracture to separation. The specimen endured an additional 4,400 cycles, less than 1% of the number of cycles endured during ultrasonic loading. Therefore, it was determined that using the number of cycles at automatic test stoppage in the USF-2000A was valid as the point of fatigue failure of the welded joints.

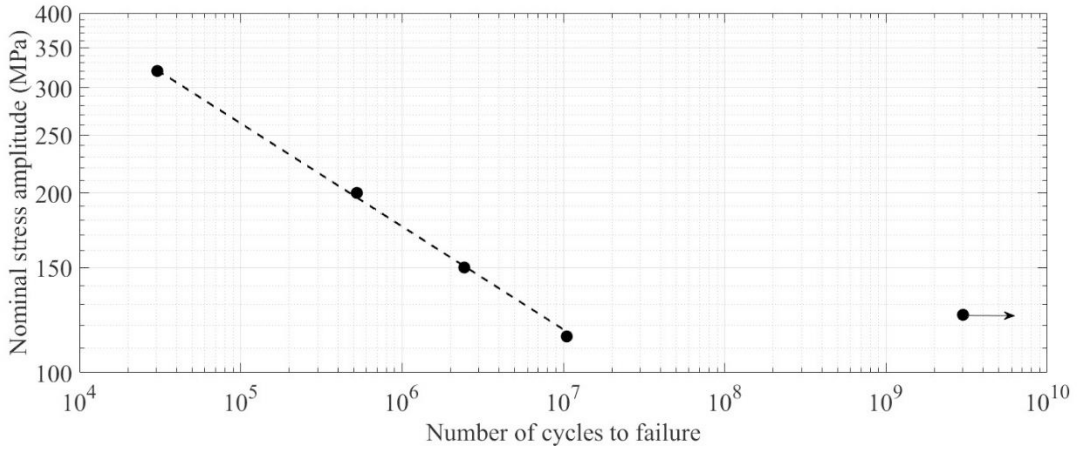

Fig. 4. Ultrasonic fatigue testing SN diagram.

3.3. Comparison to IIW design curve

The stress at the weld toe, where cracks initiated in all failed specimens, was assessed using the effective notch stress procedure following IIW guidelines (Fricke, 2008). As the thickness of the joints was < 5 mm, the modified method with the 0.05 mm reference radii at the weld toes was used (Sonsino et al., 2012). Employing a similar FEA model to that detailed in Section 2.3, but with a finer mesh, a stress concentration factor of $K_t = 3.09$ was determined. For the notch stress concept with a 0.05 mm reference radii, a FAT 560 class is used for a stress ratio of R = 0.5. A fatigue enhancement factor of 1.3 was applied, as the fatigue tests in this research were conducted at R = -1, (Hobbacher, 2016). The IIW design curve is plotted alongside the current research results and associated SN curves for a probability of survival of 50% and 95% in Fig. 5. The 95% probability of survival SN curve lies entirely above the IIW design curve, with a slight increase (12%) in fatigue strength at 2 x 10^6 cycles. The extent of the frequency effect has not been thoroughly studied for welded joints. However, considering studies of low carbon steel base material (Guennec et al., 2023), there is likely to be an increase in measured fatigue strength with UFT of this welded joint. Nevertheless, the obtained fatigue results are comparable to the IIW design curve for the effective notch stress concept.

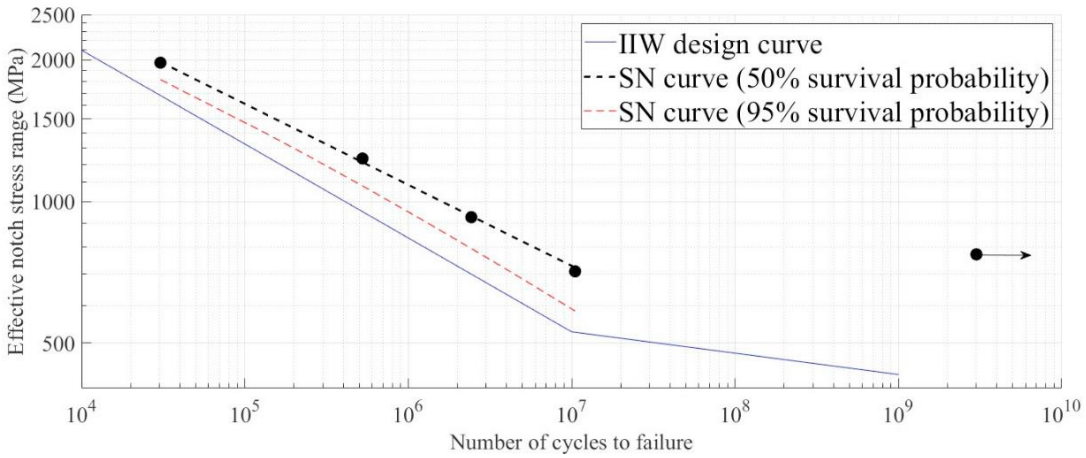

Fig. 5. SN curve for effective notch stress and comparison to IIW design curve.

3.4. Fractography

The fatigue cracks in the 4 failed specimens initiated at the weld toe, as shown in Fig. 6a. It was established that the stress concentration at the weld toe was the limiting factor on the fatigue strength of these welded specimens. Fig. 6b shows the typical fracture surface of a specimen, with the fatigue crack initiated on the specimen surface. The adjacent fatigue crack propagation region is indicated by the smooth appearance and ratchet marks. The propagation region indicated the crack growth during ultrasonic loading, which nearly extends through the full thickness in the examined specimen. The ductile failure, shown by the darker rough surface, was caused by tensile overload after fatigue testing.

One specimen was sectioned and subjected to the standard metallurgical preparation procedure to study the microstructural constituents of the crack initiation and propagation regions. The cross section, transverse to the direction of crack growth, is shown in Fig. 6c. The crack initiated at the boundary between the FZ and HAZ and propagated through the HAZ. Although the hardness of the HAZ was greater than that of the FZ, and therefore expected to have a greater fatigue strength (Casagrande et al., 2011), the effect of the stress concentration at the weld toe appears to be dominant.

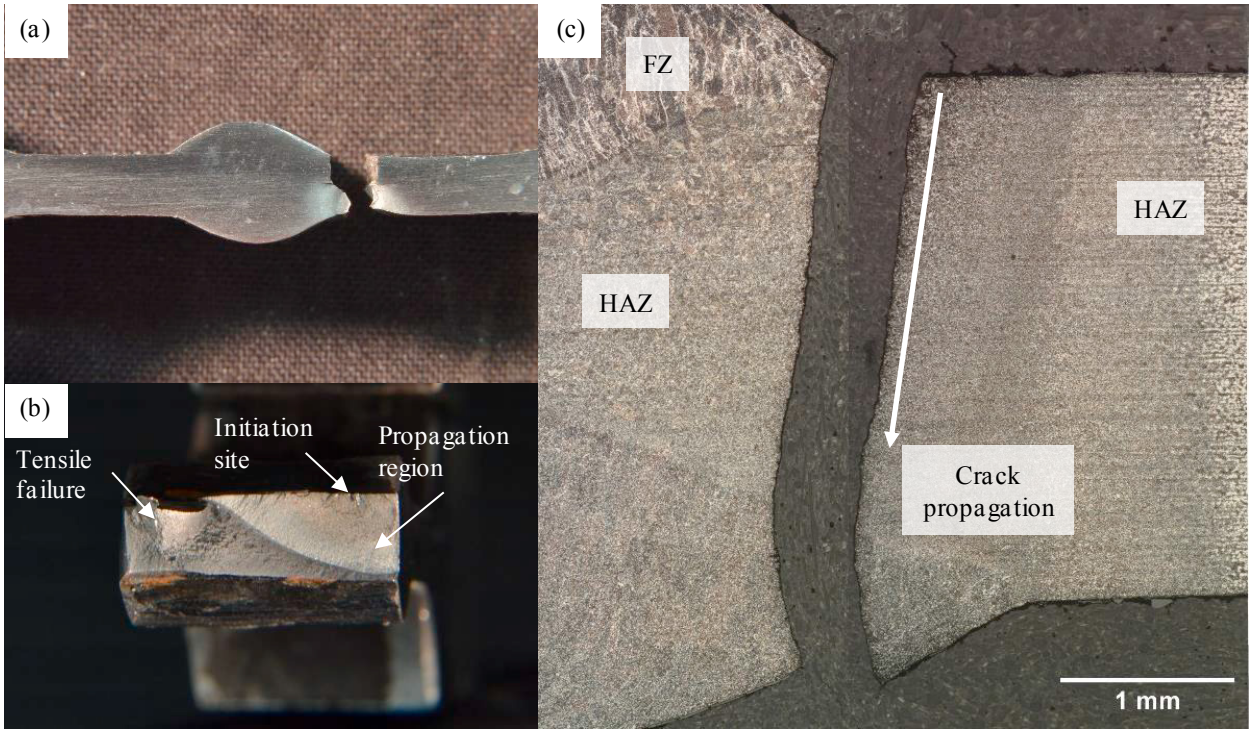

Fig. 6. Fractography of failed specimens: (a) side view showing characteristic failure from weld toe (σ_a = 320 MPa, N_f = 3.04 x 10^4); (b) fracture surface (σ_a = 150 MPa, N_f = 1.05 x 10^7); (c) cross-section transverse to crack propagation direction [x50, etched].

4. Conclusions

The proposed novel specimen design detailed herein, which included the weld toe in the region of highest stress, was shown to be suitable for UFT and studying the fatigue properties of structural steel welded joints up to the gigacycle domain. Specimens showed consistent testing characteristics and failed specimens displayed low scatter to a power fit curve. All fatigue cracks initiated from the weld toe and propagated through the HAZ. Future work will include an expanded testing regime and comparator fatigue tests with the same specimen geometry at conventional frequency (20 Hz) to assess the frequency effect with this material and welded specimen design.

References

Bathias, C., & Paris, P. C. (2005). *Gigacycle Fatigue in Mechanical Practice* (L. L. Faulkner, Ed.). Marcel Dekker.

Benscoter, A. O., & Bramfitt, B. L. (2004). Metallography and Microstructures of Low-Carbon and Coated Steels. In *ASM Handbook: Metallography and Microstructures* (pp. 588–607). ASM International. https://doi.org/10.31399/asm.hb.v09.a0003761

BS 7608. (2015). *Guide to fatigue design and assessment of steel products*. BSI Standards Publication.

Casagrande, A., Cammarota, G. P., & Micele, L. (2011). Relationship between fatigue limit and Vickers hardness in steels. *Materials Science and Engineering A*, *528*(9), 3468–3473. https://doi.org/10.1016/J.MSEA.2011.01.040

EN 10025-2. (2019). *Hot rolled products of structural steels Part 2: Technical delivery conditions for non-alloy structural steels*. European Committee for Standardization.

EN ISO 17362. (2015). *Welding consumables. Tubular cored electrodes for gas shielded and non-gas shielded metal arc welding of non-alloy and fine grain steels*. European Committee for Standardization.

Fitzka, M., Schönbauer, B. M., Rhein, R. K., Sanaei, N., Zekriardehani, S., Tekalur, S. A., Carroll, J. W., & Mayer, H. (2021). Usability of ultrasonic frequency testing for rapid generation of high and very high cycle fatigue data. *Materials*, *14*(9). https://doi.org/10.3390/ma14092245

Fricke, W. (2008). *Guideline for the fatigue assessment by notch stress analysis for welded structures*.

Fry, P. R. (2014). High cycle fatigue of welded structures: Design guidelines validated by case studies. *Engineering Failure Analysis*, *46*, 179–187. https://doi.org/10.1016/j.engfailanal.2014.08.010

Gorash, Y., Comlekci, T., Styger, G., Kelly, J., Brownlie, F., & Milne, L. (2023). Ultrasonic Fatigue Testing of Structural Steel S275JR+AR with Insights into Corrosion, Mean Stress and Frequency Effects. *Materials*, *16*(5), 1799. https://doi.org/10.3390/ma16051799

Guennec, B., Kinoshita, T., Horikawa, N., Oguma, N., & Sakai, T. (2023). Loading frequency effect on the fatigue endurance of structural carbon steels: estimation based on dislocation motion theory and experimental verification of the model. *International Journal of Fatigue*, 107634. https://doi.org/10.1016/j.ijfatigue.2023.107634

Hobbacher, A. F. (2016). Recommendations for Fatigue Design of Welded Joints and Components. In *IIW Collection* (2nd ed.). Springer. http://www.springer.com/series/13906

ISO 1099. (2017). *Metallic materials - Fatigue testing - Axial force-controlled method*. International Orginization of Standardization.

Kuhn, H., & Medlin, D. (2000). Ultrasonic Fatigue Testing. In *Mechanical Testing and Evaluation* (Vol. 8, pp. 717–729). ASM International. https://doi.org/10.31399/asm.hb.v08.a0003315

Liu, Y., He, C., Huang, C., Khan, M. K., & Wang, Q. (2014). Very long life fatigue behaviors of 16Mn steel and welded joint. *Structural Engineering and Mechanics*, *52*(5), 889–901. https://doi.org/10.12989/sem.2014.52.5.889

Phillips, D. H. (2016). *Welding Engineering: An Introduction*. Wiley.

Pu, X., Petit, J., Darbord-Ranc, I., & Wagner, D. (2019). Thermal response of iron and C-Mn steels with different ferrite/pearlite phase fraction under ultrasonic fatigue loading. *Materials Science and Engineering A*, *749*, 96–105. https://doi.org/10.1016/J.MSEA.2019.02.017

Shimadzu. (2017). *USF-2000A Hardware Instruction Manual*.

Sonsino, C. M., Fricke, W., De Bruyne, F., Hoppe, A., Ahmadi, A., & Zhang, G. (2012). Notch stress concepts for the fatigue assessment of welded joints - Background and applications. *International Journal of Fatigue*, *34*(1), 2–16. https://doi.org/10.1016/j.ijfatigue.2010.04.011

Swacha, P., & Lipski, A. (2023). Cracking of S355J2+N steel in the high-cycle and very-high-cycle fatigue regimes. *International Journal of Fatigue*, *168*, 107388. https://doi.org/10.1016/J.IJFATIGUE.2022.107388

Torabian, N., Favier, V., Dirrenberger, J., Adamski, F., Ziaei-Rad, S., & Ranc, N. (2017). Correlation of the high and very high cycle fatigue response of ferrite based steels with strain rate-temperature conditions. *Acta Materialia*, *134*, 40–52. https://doi.org/10.1016/J.ACTAMAT.2017.05.064

WES 1112. (2022). *Method for ultrasonic fatigue testing in metallic material*. Japan Welding Engineering Society.

Zhao, X., Dongpo, W., Deng, C., Liu, Y., & Zongxian, S. (2012). The fatigue behaviors of butt welds ground flush in the super-long life regime. *International Journal of Fatigue*, *36*(1), 1–8. https://doi.org/10.1016/j.ijfatigue.2011.09.009